N85-22491

CALCULATION OF SECONDARY-ELECTRON ESCAPE CURRENTS FROM INCLINED SPACECRAFT SURFACES IN A MAGNETIC FIELD*

J. G. Laframboise
York University
Toronto, Canada M3J 1P3

In low Earth orbit, the geomagnetic field $\vec{B}$ is strong enough that secondary electrons emitted from spacecraft surfaces have an average gyroradius much smaller than typical dimensions of large spacecraft. This implies that escape of secondaries will be strongly inhibited on surfaces which are nearly parallel to $\vec{B}$, even if a repelling electric field exists outside them. This effect is likely to make an important contribution to the current balance and hence the equilibrium potential of such surfaces, making high-voltage charging of them more likely. We present numerically-calculated escaping secondary electron fluxes for these conditions. For use in numerical spacecraft-charging simulations, we also present an analytic curve-fit to these results, accurate to within 3% of the emitted current.

1. INTRODUCTION

The prediction of high-voltage charging or other environmental effects on a spacecraft in low Earth orbit appears likely to be more complicated than in geostationary orbit, for at least three reasons.

These reasons are: (a) space charge effects (on sheath and wake potentials) are more important, because space-charge densities are much higher (the Debye length is no longer >> typical spacecraft dimensions) (b) ion flow effects are more important, because spacecraft orbital speed $\gtrsim$ ion thermal speeds (c) the geomagnetic field $\vec{B}$ is likely to have an important influence on charged-particle motions because $\vec{B}$ is now much larger, and not all of the average particle gyroradii of importance are any longer >> typical spacecraft dimensions.

We wish to investigate an important consequence of (c), which concerns the escape of secondary electrons emitted from spacecraft surfaces. Our discussion will also apply, with minor modifications, to photoelectron or backscattered-electron escape. In low Earth orbit, in the auroral-zone geomagnetic field ($|\vec{B}| = 0.44$ gauss $= 4.4 \times 10^{-5}$T), the gyroradius of a "typical" 3eV secondary electron and a 10 keV auroral electron are 13 cm and 8 m, respectively. The average gyroradius of "cold" ionospheric electrons (temperature T = 0.1 eV) in the same $\vec{B}$ is even smaller (2 cm), but this is not an important parameter in most cases because these electrons are repelled if the spacecraft potential is negative, and their density is then well-approximated by a Boltzmann factor, which is unaltered by $\vec{B}$ effects.

The reason why $\vec{B}$ affects secondary-electron escape is shown in Fig. 1. In Fig. 1(a), the spacecraft surface is perpendicular to $\vec{B}$, and the emitted electrons, which

* Work supported by the United States Air Force under Contract No. F19628-83-K-0028.

experience an electric force $-e\vec{E}$ directed away from the surface, all escape, helping to discharge it. In Fig. 1(b), the spacecraft surface is nearly parallel to $\vec{B}$, and almost all of the emitted electrons return to it, even though they still experience an electric force directed away from it. These electrons therefore are unable to help discharge it, so a surface nearly parallel to $\vec{B}$ is more likely to charge to a large negative voltage. Note that the component of $\vec{E}$ which is perpendicular to $\vec{B}$ results only in an $\vec{E} \times \vec{B}$ drift parallel to the surface.

For any object much larger than 13 cm, the escape of secondary electrons will be strongly affected by this process. For example, most surfaces on the Shuttle are effectively "infinite planes" by this criterion. On the other hand, the average gyroradius of high-energy auroral electrons is comparable to Shuttle dimensions, so the deposition of these electrons onto Shuttle surfaces is likely to be only moderately inhibited.

For a larger object (size >> 8 m), deposition of auroral electrons will also become strongly orientation-dependent, with both collection and escape of electrons now being inhibited on surfaces nearly parallel to $\vec{B}$. This suggests that high-voltage charging of such surfaces may be more likely on objects of intermediate size than on either larger or smaller ones. In the calculation of Parks and Katz[1], Katz and Parks[2], the tendency toward high-voltage charging increased with spacecraft size because in their model, ion collection increased less rapidly with spacecraft size than did electron collection. To determine which of these two effects predominates will require more detailed calculations than have been done so far.

As already mentioned, strong ion flow effects also are generally present in low orbit; the ion speed ratios (flow speed/most probable ion thermal speed) for H^+ at 1 keV, H^+ at 0.1 eV, and O^+ at 0.1 eV are 0.02, 1.8, and 7.3, respectively. Whenever the latter is the predominant ion species, ion collection on downstream surfaces will therefore be strongly inhibited. If a surface is simultaneously downstream and nearly parallel to $\vec{B}$, as is likely to be the case in the auroral zones, then the tendency for high-voltage charging to occur on it will be greatly increased (Fig. 2).

To "straightforwardly" include $\vec{B}$ effects on secondary electron emission in a large two or three dimensional simulation program would involve the numerical integration of very large numbers of secondary-electron orbits. The resulting computing costs usually would be formidable, especially since these orbits would have relatively large curvatures. A desirable alternative is to "parameterize" the situation by treating in advance a simplified but still sufficiently realistic model problem. In order to do this, we make the approximations described in the next Section.

2. THEORY FOR $\vec{E}$ NORMAL TO SURFACE

We assume that the spacecraft surface is an infinite plane, and the electric and magnetic fields $\vec{E}$ and $\vec{B}$ outside it are uniform. In the work presented here, we also assume that the electric force $-e\vec{E}$ on electrons is directed along the outward normal to the surface; here e is the magnitude of the elementary charge. This assumption is to be relaxed in a later paper (J.G. Laframboise, to be published) in order to permit variations of potential along the surface to be taken into account. We assume that the secondary electrons are emitted with a Maxwellian distribution corresponding to a temperature T. The ratio $i = I/I_o$ of escaping to emitted flux is then a function of two parameters: the angle θ between the surface normal and the direction of $\vec{B}$ (Fig.3), and a parameter describing the strength of $\vec{E}$. A convenient choice for this parameter is the difference in potential across a mean secondary-electron gyroradius $\bar{a} = (1/eB)(\pi mkT/2)^{\frac{1}{2}}$, divided by kT/e, where m is electron mass and k is Boltzmann's constant.

This quotient is:

$$\epsilon \equiv \frac{E}{B}\sqrt{\frac{\pi m}{2kT}} \tag{2.1}$$

where $E \equiv |\vec{E}|$ and $B \equiv |\vec{B}|$.

This quantity also has an alternative, more useful interpretation: it is the ratio of the magnitude $|\vec{E}\times\vec{B}|/B^2$ of the $\vec{E}\times\vec{B}$ drift speed, to one-half the mean thermal speed $(8kT/\pi m)^{1/2}$ of the emitted electrons. It is useful to estimate the value of ϵ for a high-voltage spacecraft sheath in low-orbit conditions. To do this, we use the sheath solution of Al'pert et al (Ref. 3, Table XXIV and Fig. 72). For a 1 kV and a 5 kV sheath around a sphere of radius 3m in a collisionless plasma having an ambient ion temperature of 0.1V, number density of 3×10^5 cm^{-3}, and resultant (ion) Debye length of 0.43 cm, their results give, respectively, sheath thicknesses of 2.6 and 6.1 m, and surface electric fields E = 0.86 and 2.9 kV/m. Using $B = 4.4\times10^{-5}$T and T = 3 eV for secondary electrons, we then obtain ϵ = 33.9 and 114.2. Both of these are relatively large values, whose significance can be understood if we consider what would happen if ϵ were infinite.

In this limit, it is easy to show that secondary electrons would all escape unless $\vec{B}$ were exactly parallel to the surface (θ were 90°). This can be shown as follows. In this limit, secondary electrons would have no "thermal" motion. The (y,z) projection of their motion would then be similar to that shown in Fig. 4. This motion would be the sum of: (i) an $\vec{E}\times\vec{B}$ drift in the y direction (ii) a uniform acceleration along $\vec{B}$, whose projection in the (y,z) plane would be upward (iii) just enough gyromotion to produce a cycloidal path when combined with (i), so that in the absence of (ii), the electron would (just) return to the surface at the end of each gyroperiod. In the presence of (ii), these "return points" are displaced upward by progressively increasing amounts (Fig. 4), so the electron can never return to the surface, unless $\vec{B}$ is exactly parallel to the surface, so that the upward component of $-e\vec{E}$ along $\vec{B}$ vanishes.

This result suggests that for large finite values of ϵ (including the values calculated above), electron escape is likely to be almost complete except for θ very near 90°, where it should drop to zero very steeply. The occurrence of high-voltage charging in marginal circumstances may therefore depend very strongly on the precise orientation of a surface.

The escaping secondary-electron flux is given by:

$$\begin{aligned} I &= \iiint f(\vec{v}_o)H(\vec{v}_o)v_{oz}\,d^3\vec{v}_o \\ &= \int_{-\infty}^{\infty}dv_{ox}\int_{-\infty}^{\infty}dv_{oy}\int_0^{\infty}n\left(\frac{m}{2\pi kT}\right)^{3/2}\exp\left(-\frac{mv_o^2}{2kT}\right)H(v_{ox},v_{oy},v_{oz})v_{oz}\,dv_{oz} \end{aligned} \tag{2.2}$$

where: $\vec{v}_o$ is the initial velocity of an emitted electron, $f(\vec{v}_o) \equiv d^3n/d^3\vec{v}_o$ is the velocity distribution of emitted electrons, n is a reference number density, and $H(\vec{v}_o)$ is equal to 1 for escaping electrons and 0 for those which return to the surface. The emitted flux is:

$$I_o = n(kT/2\pi m)^{1/2}. \tag{2.3}$$

We also introduce the dimensionless velocity:

$$\vec{u} = \vec{v}(m/2kT)^{1/2}. \tag{2.4}$$

Equation (2.2) then becomes:

$$\frac{I}{I_o} = \frac{2}{\pi}\int_{-\infty}^{\infty}\int_{-\infty}^{\infty} du_{ox}du_{oy}e^{-u_{ox}^2-u_{oy}^2}\int_0^{\infty} du_{oz}\, u_{oz}\, e^{-u_{oz}^2}\, H(u_{ox},u_{oy},u_{oz})$$

$$= \frac{1}{\pi}\int_{-\infty}^{\infty}\int_{-\infty}^{\infty} du_{ox}\, du_{oy}\exp(-u_{ox}^2-u_{oy}^2)\sum_{k=1}^{k_{max}(u_{ox},u_{oy})}(-1)^{k+1}\exp\left[-u_{lim,k}^2(u_{ox},u_{oy})\right]$$

$$\approx \frac{1}{\pi}\sum_i\sum_j \Delta u_{ox}\Delta u_{oy}\exp(-u_{ox,i}^2-u_{oy,j}^2)\sum_{k=1}^{(k_{max})i,j}(-1)^{k+1}\exp\left[\left(-u_{lim,k}^2\right)i,j\right] \qquad (2.5)$$

which is in a form suitable for numerical summation. The quantities $u_{lim,1}, u_{lim,2}, \ldots, u_{lim,k_{max}}$ are the values of u_{oz} for which H changes between 0 and 1 for each u_{ox} and u_{oy}. These values must be found by numerically determining which particle orbits reimpact the surface. These orbits can, however, be determined in analytic form, with time as a parameter. To do this, we use the coordinate system shown in Fig. 3, together with a y-axis (not shown) directed into the plane of the Figure. The equation of motion for an electron is:

$$\dot{\vec{v}} = -\frac{e}{m}(\vec{E}+\vec{v}\times\vec{B}). \qquad (2.6)$$

We solve this with the initial conditions $\xi = y = \eta = 0$, $v_\xi = v_{o\xi}$, $v_y = v_{oy}$, and $v_\eta = v_{o\eta}$. We introduce the dimensionless variables:

$$\varepsilon_x = \frac{E_x}{B}\sqrt{\frac{\pi m}{2kT}}, \quad \varepsilon_y = \frac{E_y}{B}\sqrt{\frac{\pi m}{2kT}}, \text{ etc;}$$

$$\tilde{x} = x/\bar{a}, \ \tilde{y} = y/\bar{a}, \text{ etc;} \qquad (2.7)$$

$$\tau = \omega_c t = (eB/m)t.$$

In the present work, ε_x and ε_y are both zero, but for future use, we have retained these quantities in the formulas below. We obtain:

$$u_{o\xi} = u_{ox}\sin\theta + u_{oz}\cos\theta;$$
$$u_{o\eta} = -u_{ox}\cos\theta + u_{oz}\sin\theta;$$
$$\tilde{\xi} = -\frac{1}{\pi}\varepsilon_\xi\tau^2 + \frac{2}{\sqrt{\pi}}u_{o\xi}\tau;$$
$$\tilde{y} = \left(\frac{2}{\sqrt{\pi}}u_{oy} - \frac{2}{\pi}\varepsilon_\eta\right)\sin\tau + \left(\frac{2}{\sqrt{\pi}}u_{o\xi} + \frac{2}{\pi}\varepsilon_y\right)(\cos\tau - 1) + \frac{2}{\pi}\varepsilon_\eta\tau;$$
$$\tilde{\eta} = \left(\frac{2}{\sqrt{\pi}}u_{o\eta} + \frac{2}{\pi}\varepsilon_y\right)\sin\tau + \left(\frac{2}{\sqrt{\pi}}u_{oy} - \frac{2}{\pi}\varepsilon_\eta\right)(1-\cos\tau) - \frac{2}{\pi}\varepsilon_y\tau; \qquad (2.8)$$
$$\tilde{z} = \tilde{\xi}\cos\theta + \tilde{\eta}\sin\theta.$$

Equations (2.8) can also be differentiated to find $d\tilde{z}/d\tau$. The numerical procedure for finding the quantities $u_{lim,k}$ in Eq. (2.5) then involves calculating $\tilde{z}$ and $d\tilde{z}/d\tau$ at a succession of points along an orbit (the electron will reimpact during the first gyroperiod $0 < \tau \leq 2\pi$ if at all, so this interval always suffices), and making the appropriate tests on these quantities to find out whether the orbit reimpacts or escapes. For each $u_{ox,i}$ and $u_{oy,j}$, this is done for a succession of values of u_{oz}. These tests also yield the local minimum of $\tilde{z}(\tau)$ if one exists. Whenever a change occurs between nc escape and escape from one such value of u_{oz} to the next, an interpolation using these minima can be used to provide the corresponding value of

$u_{lim,k}$. In cases where they are unavailable, the arithmetic mean of the two successive u_{oz} values is used. This completes the definition of the procedure used for calculating the ratio I/I_c of escaping to emitted flux.

3. RESULTS AND DISCUSSION

Escaping secondary-electron current densities, computed as described in Sec. 2, are shown in Table 1 and Fig. 5. Each value of $i = I/I_o$ was calculated using 191808 orbits, evenly spaced in the intervals $-4.5 \leq u_{ox} \leq 4.5$, $-4.5 \leq u_{oy} \leq 4.5$, and $0 \leq u_{oz} \leq 4.5$, with points on the orbits calculated at intervals $\Delta\tau = \pi/45$. For 8 values each of ε and θ, the resulting calculation took 83 hr total on a Hewlett-Packard 1000F minicomputer with Vector Instruction Set. The results are accurate to within about 0.5% or better. The result for $\varepsilon = 0$ is just the analytic result $i = \cos\theta$. To see why this is so, we consider the electron orbit shown in Fig. 6, which has been fictitiously extended so as to pass through the surface and re-emerge from it. In the absence of an electric field ($\varepsilon = 0$), this orbit has the same speed at the re-emergence point C as at the emission point A. Since we have also assumed that the emitted velocity distribution is isotropic, and therefore a function of speed only, the real orbit, for which C is the emission point, must carry the same population as would the fictitious re-emerged orbit. The flux crossing the reference surface DE, which is $\perp \vec{B}$, is therefore the same as if such passages and re-emergences actually occurred, and is the same as if another reference surface FG, also $\perp \vec{B}$, were emitting electrons having the same velocity distribution. However, in reality, the electrons come from the real surface HJ, which is not $\perp \vec{B}$, and all the electron-orbit guiding centers which are inside any given magnetic-flux tube through DE will also be inside the projection of the same flux tube onto HJ, and the ratio of the intersection areas of this tube with HJ and DE is just $\sec\theta$. The ratio of escaping to emitted flux must therefore be the reciprocal of this, or $\cos\theta$, as stated above.

Also evident in Fig. 5 is the fact, mentioned in Sec. 2, that when ε is large enough, electron escape becomes essentially complete except when θ is very nearly 90°. In a real situation, $\vec{E}$ would not be uniform, but would decrease with distance from the surface, contrary to our assumptions. Our results can therefore be expected to overestimate electron escape. This would probably not be a large effect, but this presumption remains to be verified. An approximate compensation for it can be made by calculating ε using an electric field value which is averaged over the first mean gyroradius distance from the surface.

The results in Table 1 are approximated to within 2.5% of I_o by the empirical formula:

$$
\begin{aligned}
a &= 1 + 1.35\varepsilon^{1.1394} \exp\left\{0.083725\left\{1 + \tanh\left[1.9732 \ln\left(\frac{\varepsilon}{1.13}\right)\right]\right\}\right. \\
&\quad \left. - 0.07825 \ln\left[1 + (\varepsilon/8.5)^{1.78148}\right]\right\}; \\
b &= 0.38033\varepsilon^{0.95892} \exp\left\{2.0988\left\{1 + \tanh\left[1.49 \ln\left(\frac{\varepsilon}{3.26}\right)\right]\right\}\right\}; \\
c &= \ln(90^\circ/\theta); \qquad (3.1) \\
i &= \cos\left[90^\circ \exp(-ac - bc^2)\right].
\end{aligned}
$$

This formula also has the correct limiting behavior when $\varepsilon \to 0$ or ∞, or $\theta \to 0^\circ$ or 90°.

An approximation formula for the emitted flux is also available [Eqs. (5) and

(6) of Laframboise et al, Ref. 4, and Laframboise and Kamitsuma, Ref. 5].

4. CALCULATION OF SECONDARY-ELECTRON DENSITIES

Once the secondary-electron escape fluxes are known (Sec. 3), a simple, inexpensive, approximate calculation of their space-charge density distribution can be set up. The proposed method is as follows: (1) ignore the gyromotion of the secondary electrons once they have escaped. Their motion then involves: (a) an acceleration along magnetic field lines, of amount $-(e/m)\vec{E}\cdot\vec{B}/B$ (b) a drift motion of velocity $\vec{E}\times\vec{B}/B^2$ across magnetic field lines. (2) Integrate enough of the trajectories defined by this motion (i.e. their guiding-center trajectories) to define trajectory tubes whose cross-section at any point can be calculated with sufficient accuracy; the method described by Laframboise et al (Ref. 6, Sec. 7), can be used to calculate the area of a trajectory tube without reference to neighbouring trajectories. (3) Calculate their space-charge density $n(\vec{r})$ at any point by (a) ignoring the "thermal" spread of their velocities (b) then invoking the fact that their density × their velocity [as given by the orbit integration mentioned in (2)], × the cross-sectional area $A(\vec{r})$ of the trajectory tube (which must be calculated in a plane ⊥ the trajectory) at the point $\vec{r}$ in question, = a constant (whose value is given by the initial conditions at the point on the spacecraft where the trajectory originates) (c) finding their velocity at the point in question by using energy conservation, together with the values of electric potential $\phi(\vec{r})$ and ϕ_o at that point and the emission point, and their assumed velocity v_o at the emission point. The result is:

$$n(\vec{r}) = n_o v_o A_o \Big/ \left\{ A(\vec{r}) \sqrt{v_o^2 + (2e/m)\left[\phi(\vec{r}) - \phi_o\right]} \right\} \tag{4.1}$$

where $n_o v_o$ is the escaping flux calculated in Sec. 3. At most positions, $n(\vec{r})$ will be insensitive to the precise value assumed for v_o^2; assuming that v_o = the one-sided thermal speed $(2kT/\pi m)^{\frac{1}{2}}$ will suffice for most purposes.

REFERENCES

1. Parks, D.E., and Katz, I. (1981) Charging of a large object in low polar Earth orbit. In: Spacecraft Charging Technology 1980, NASA Conference Publication 2182/Report No. AFGL-TR-81-0270, Air Force Geophysics Laboratory, Massachusetts, pp. 979-989.
2. Katz, I., and Parks, D.E. (1983) Space shuttle orbiter charging. J. Spacecraft and Rockets 20, 22-25.
3. Al'pert, Ya.L., Gurevich, A.V., and Pitaevskii, L.P. (1965) Space Physics with Artificial Satellites, Consultants Bureau, New York.
4. Laframboise, J.G., Kamitsuma, M., and Godard, R. (1982) Multiple floating potentials, "threshold-temperature" effects, and "barrier" effects in high-voltage charging of exposed surfaces on spacecraft. In: Proc. Internat. Symp. on Spacecraft Materials in Space Environment, June 1982, Toulouse, France, European Space Agency, Paris, Publication No. ESA SP-178, pp. 269-275.
5. Laframboise, J.G., Kamitsuma, M. (1983) The threshold temperature effect in high-voltage spacecraft charging. In: Proc. Air Force Geophys. Lab. Workshop on Natural Charging of Large Space Structures in Near Earth Polar Orbit, edited by R.C. Sagalyn, D.E. Donatelli, and I. Michael, Report No. AFGL-TR-83-0046/ Environmental Research Paper No. 825, Air Force Geophysics Laboratory, Massachusetts, pp. 293-308.
6. Laframboise, J.G., Kamitsuma, M., Prokopenko, S.M.L., Chang, Jen-Shih, and Godard, R. (1982) Numerical Simulation of spacecraft charging phenomena at high altitude, Final Report on Grant AFOSR-76-2962, York University.

EPS \ THETA	15.00	30.00	45.00	60.00	75.00	80.00	85.00	89.00
0.00	.965	.866	.707	.500	.259	.173	.087	.017
.20	.991	.934	.796	.585	.311	.209	.105	.020
.50	.999	.976	.878	.704	.392	.271	.137	.027
1.00	.999	.992	.971	.859	.545	.384	.190	.039
2.00	.999	1.000	.999	.982	.802	.617	.342	.070
5.00	.999	1.000	1.000	1.000	.998	.960	.784	.172
10.00	.999	1.000	1.000	.999	1.000	1.000	.971	.330
20.00	.999	1.000	1.000	.999	1.000	1.000	1.000	.619

TABLE 1

Values of the ratio $i = I/I_o$ of escaping to emitted flux, for various values of θ, the angle (in degrees) between the surface normal and the magnetic field direction, and ε, the nondimensional repelling electric field strength. These two quantities appear in the table as THETA and EPS, respectively. These results are accurate to within about 0.5% or better; thus the differences between .999 and 1.000 in the Table are not significant. For $\theta = 0^o$, $i = 1$ for all values of ε.

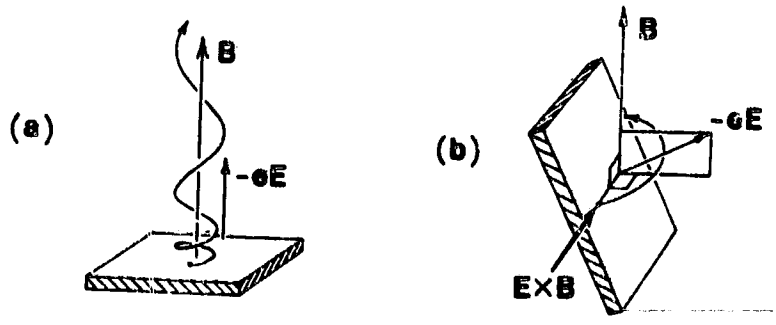

Figure 1. Effect of surface orientation on escape of emitted electrons. In (a), the spacecraft surface is perpendicular to the magnetic field $\vec{B}$, and the emitted electrons, which experience an electric force $-e\vec{E}$ directed away from the surface, all escape. In (b), the spacecraft surface is nearly parallel to $\vec{B}$, and almost all of the emitted electrons return to the surface, even though they still experience an electric force directed away from it. Note that the component of $\vec{E}$ perpendicular to $\vec{B}$ results only in an $\vec{E} \times \vec{B}$ drift parallel to the surface.

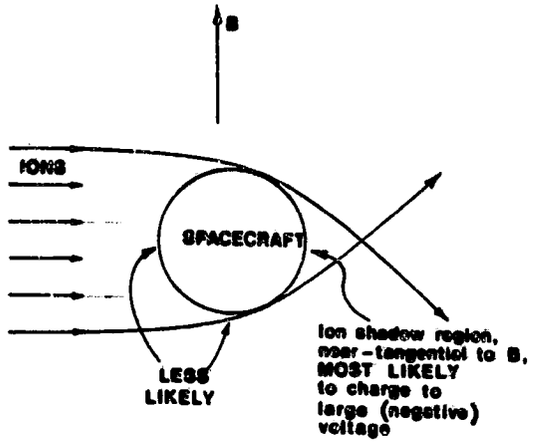

Figure 2. Spacecraft simultaneously in a collisionless ion flow and a magnetic field $\vec{B}$.

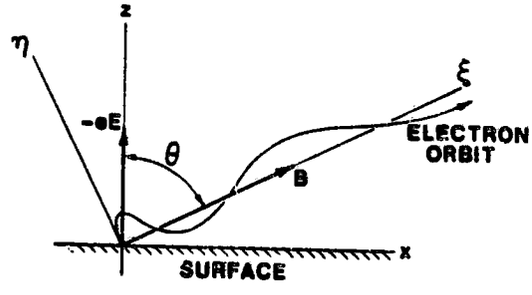

Figure 3. Coordinate system for calculating electron escape fluxes. The y-coordinate (not shown) is directed into the plane of the Figure.

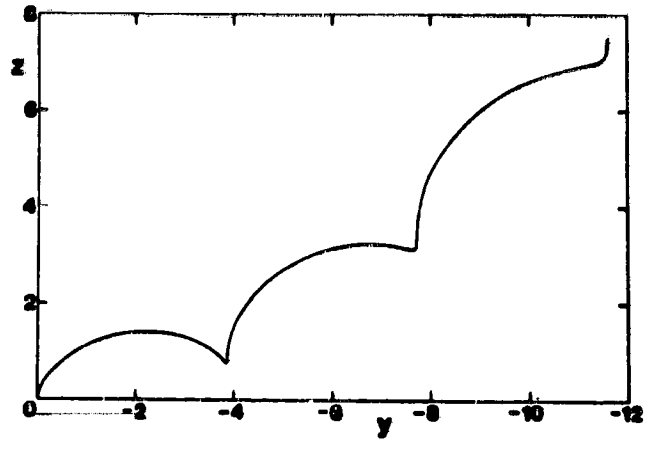

Figure 4. Example of an electron orbit having zero initial velocity. The magnetic field $\vec{B}$ is parallel to the (x,z) plane, and makes an angle $\theta = 75^{\circ}$ with the z axis. $\varepsilon = 1$. Three gyroperiods of the orbit ($0 \leq \tau \leq 6\pi$) are shown.

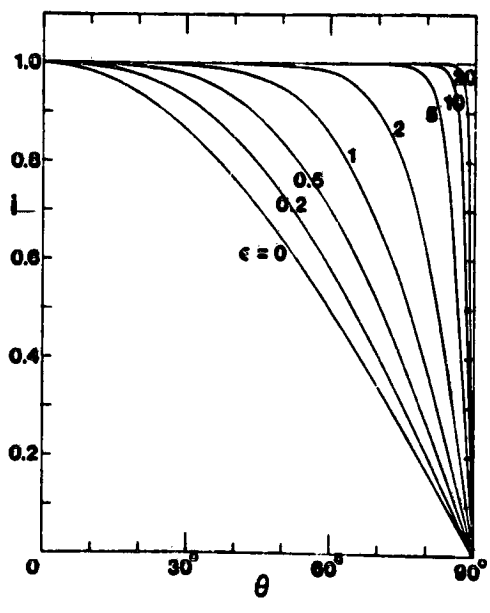

Figure 5. Ratio $i = I/I_0$ of escaping to emitted secondary-electron flux, as a function of the angle θ between the surface normal and the magnetic field direction, for various values of the repelling electric field strength parameter $\varepsilon = (E/B)(\pi m/2kT)^{\frac{1}{2}}$. The result for $\varepsilon = 0$ is given by $i = \cos\theta$.

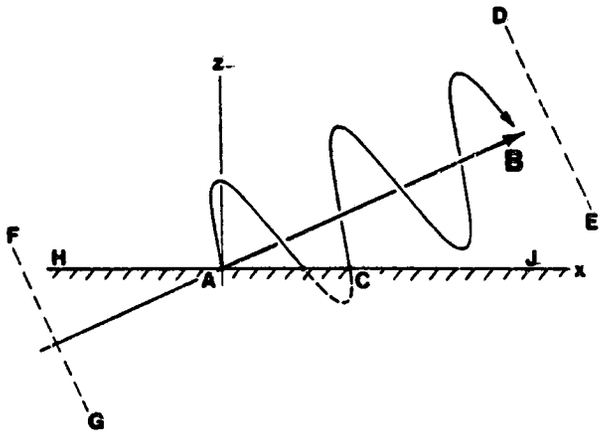

Figure 6. Electron orbit for $\varepsilon = 0$, fictitiously extended so as to pass through the surface and re-emerge from it.